SINERGI Vol. 27, No. 1, February 2023: 1-6
http://publikasi.mercubuana.ac.id/index.php/sinergi
http://doi.org/10.22441/sinergi.2023.1.001

High-temperature failure of steel boiler tube secondary superheater in a power plant

Sulthoni Akbar[1,2], Desrilia Nursyifaulkhair[2], Leanddas Nurdiwijayanto[3], Alfian Noviyanto[2,4*], Nurul Taufiqu Rochman[5]
[1]Departement of Industrial Engineering, Faculty of Engineering, University of Nahdlatul Ulama Indonesia, Indonesia
[2]Nano Center Indonesia, Indonesia
[3]International Center for Materials Nanoarchitectonics (WPI-MANA), National Institute for Materials Science (NIMS), Japan
[4]Department of Mechanical Engineering, Faculty of Engineering, Universitas Mercu Buana, Indonesia
[5]Research Center for Advanced Materials, National Research and Innovation Agency (BRIN), Indonesia

Abstract
This work investigated the failure analysis of the boiler tube secondary superheats in a power plant utility. The tube was composed of low carbon steel with 2.25Cr-1Mo addition, which was ruptured after a 26 h working test. The investigation of the tube's failure was performed through several analysis, such as microstructure, elemental analysis, and mechanical test. It was found the abrupt increase in the operating temperature as the primary factor of the material degradation of the tube. The microstructure analysis shows the existence of elongated grain with the formation of microcracks on the grain boundaries, indicating the exceeded stress applied in the material. The hoop stress in the ruptured tube was 42.47 MPa, which is higher than the allowable stress of 23.5 MPa at 605 °C. Furthermore, the equiaxed grain was observed in the unruptured tube, implying the microstructural change after exposure at high temperatures.

Keywords:
Boiler;
Degradation;
Hoop stress;
Microstructure;
Ruptured;

Article History:
Received: January 12, 2022
Revised: May 3, 2022
Accepted: May 13, 2022
Published: February 2, 2023

Corresponding Author:
Alfian Noviyanto,
Mechanical Engineering Department, Universitas Mercu Buana, Indonesia
Email:
alfian.noviyanto@mercubuana.ac.id
or
a.noviyanto@nano.or.id

INTRODUCTION

The boiler becomes the most crucial part of a thermal power plant, as it accounts for up to 20% of the total manufacturing cost [1]. As a vital process, its failure will cause sudden great damage and high expenses to recover the assets and personnel [2]. Furthermore, material failure in the boiler tube primarily caused a forced shutdown of the power boilers [3][4]. Therefore, preventing material degradation of the boiler tube is highly required to minimize economic loss.

Various failure cases of the tube material have been reported earlier, whereas mainly caused by corrosion [5]. For example, Varma and Yadavalli reported the welding failure in reheater tube with 500 MW was damaged after maximum operation time at 224 hours [6]. The material applied for tube-to-tube weld in reheater tube leakage consisted of the alloy of steel and stainless steel. The metal temperature is able in range 548-568°C, above the operation condition of boiler in 525°C.

Furthermore, the severe degradation happened while the microhardness value was in range 114-117HV0.5, under the requirement 160HV0.5 for fresh tube. The initial microhardness for this alloy weld achieved 209-213HV0.5, reflecting in each base metal hardness (150-153 and 222-225HV0.5 for steel and stainless steel, respectively). On the other hand, Liu et al. reported the failure of the rear water wall tube of the boiler due to the wall thinning [7]. Wall thinning occurred due to the fly-ash erosion and creep at elevated temperatures. Another case was reported a failure on the boiler tube secondary superheater due to short-term overheating [8]. The overheating was caused by

a massive clinker, originating from the concentrated and localized flue gas flow. Since the clinker was not able to transfer the heat, overheating was favored to occur, which subsequently failed the tube. Furthermore, Abouswa and Elshawesh explained that the superheater material tube's degradation occurred in the boiler, owing to the corrosion attack by the dissolved sodium hydroxide combined with high residual stress in the caustic attack area [9][10]. Another failure in boiler were caused by the hydrogen attack [11, 12, 13, 14].

Boiler shutdown was experienced by the thermal power plant company in Suryalaya, Indonesia due to the ruptured tube, as shown in Figure 1. Therefore, this research aims to investigate the cause of ruptured tube on a boiler secondary superheater (SSH) unit and to understand the failure (open rupture) mechanisms that resulted in the termination of the operation of the boiler.

METHOD

The ruptured tube used in this study was SA-213 T22, low carbon steel with the addition of 2.25Cr-1Mo (wt.%). For comparison, a new tube was also examined thoroughly as the standard. The burst boiler tube was observed and analyzed at the three different locations (points A, B, C), as shown in Figure 1. Point A was located in the wide crack of the burst area, which is known as fish mouth opening failure [15,16]. Point B was set ± 20 cm from the burst area, and 3 cm from the final crack location. Meanwhile, point C was placed in the crack-free area. The tube was cut at points A, B, and C for the microstructural and mechanical properties examinations.

The specimens were successively mounted, mechanically polished, and chemically etched using 5% nital solution for the microstructural analysis. Optical microscope (OM) and scanning electron microscope (SEM, JEOL, 6510LA) observations were performed at points A, B, and C of the ruptured tube and the standard tube. On the other hand, the chemical composition of the specimens was analyzed using energy dispersive spectroscopy (EDS). For mechanical properties analysis, hardness and tensile testing were conducted. The hardness of the specimens was examined using the Hardness Brinell (HB) method (loading of 187.5 kgf, indenter diameter of 2.5 mm); meanwhile, the strength of the specimens was measured using UPM 100 tensile test machine. Moreover, stress analysis was carried out by evaluating the Hoop stress using (1) [5].

$$\sigma_h = (p_i - p_e)\frac{D}{2t} \quad (1)$$

where σ_h is hoop stress, p_i and p_e are internal and external pressure, respectively, D is the diameter of the tube, and t is the thickness of the tube. Herein, Hoop stress is defined as stress that works tangentially towards the slice line of the tube.

RESULTS AND DISCUSSION

Table 1 compares the chemical composition between the ruptured and the standard tube. It can be seen the chemical composition of the ruptured specimen closely resembled the standard specimen. The result reveals that the failure was not related to the composition mismatch.

Figure 2 shows the microstructure of the ruptured specimens and the standard tubes obtained by the optical microscope. As observed in Figure 2 (a), point A exhibited a lamellar structure due to elongation of the grain. The lamellar microstructure consisted of ferrite (white/gray) and pearlite (black) phase, similar to those in the standard tube (Figure 2 (d)). However, the standard tube exhibited the equiaxed grain.

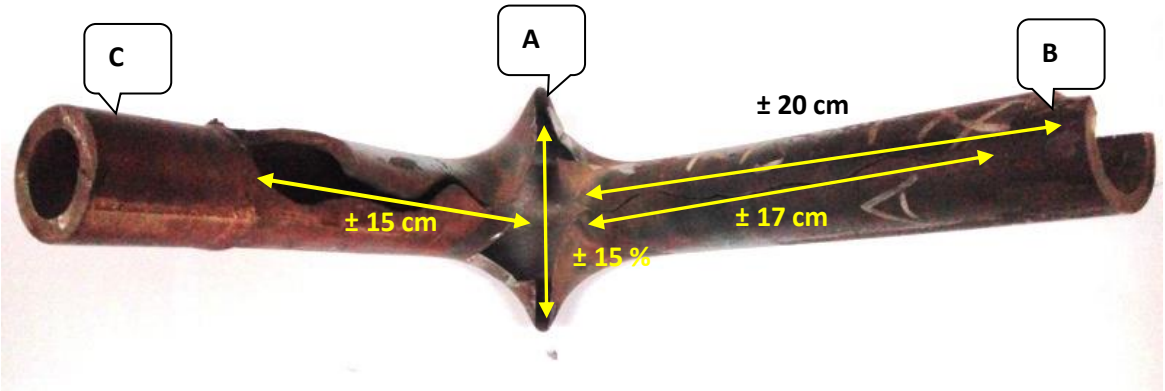

Figure 1. Image of a ruptured tube, including the location of points A, B and C.

Table 1. Chemical composition of the standard and the ruptured tube specimens

Tube	C	Si	S	P	Mn	Cr	Mo
Standard	0.05 – 0.15	< 0.5	< 0.025	< 0.025	0.3 – 0.6	1.9 – 2.6	0.87 – 1.13
Rupture	0.096	0.289	0.003	0.009	0.482	2.021	0.940

The microstructure of point B in Figure 2 (b) also displayed the lamellar grain. The grain similarity of points A (burst area) and B (near the crack area) results from the applied high stress, which consequently deformed the grains. Furthermore, the aspect ratio of the grain in point A was calculated as higher than that in point B, which indicated higher stress in point A. On the other hand, the grain shape at point C (Figure 2 (c)) is quite similar to that of the standard tube (Figure 2 (d)), suggesting lower applied stress in this point.

According to the optical microscope observation, it can be implied there is a dependency of grain shape toward the different locations, wherein the more elongated grain was found in the crack area. The elongated grains indicated that the grain experienced severe deformation due to high stress [17-20].

The mechanical properties of all specimens are summarized in Table 2. The hardness value at point A was 213 ± 25 HB, which was higher than the standard tube (163 HB). This increase can be attributed to the microstructural change from the equiaxed to the elongated grain, as shown in Figure 2. This result is in agreement with Casagrande et al. that the hardness value was changed due to microstructural alteration [21]. Moreover, the yield and tensile strength of the ruptured tube were found to be higher than that of the standard tube, as shown in Table 2, which was consistent with the hardness values.

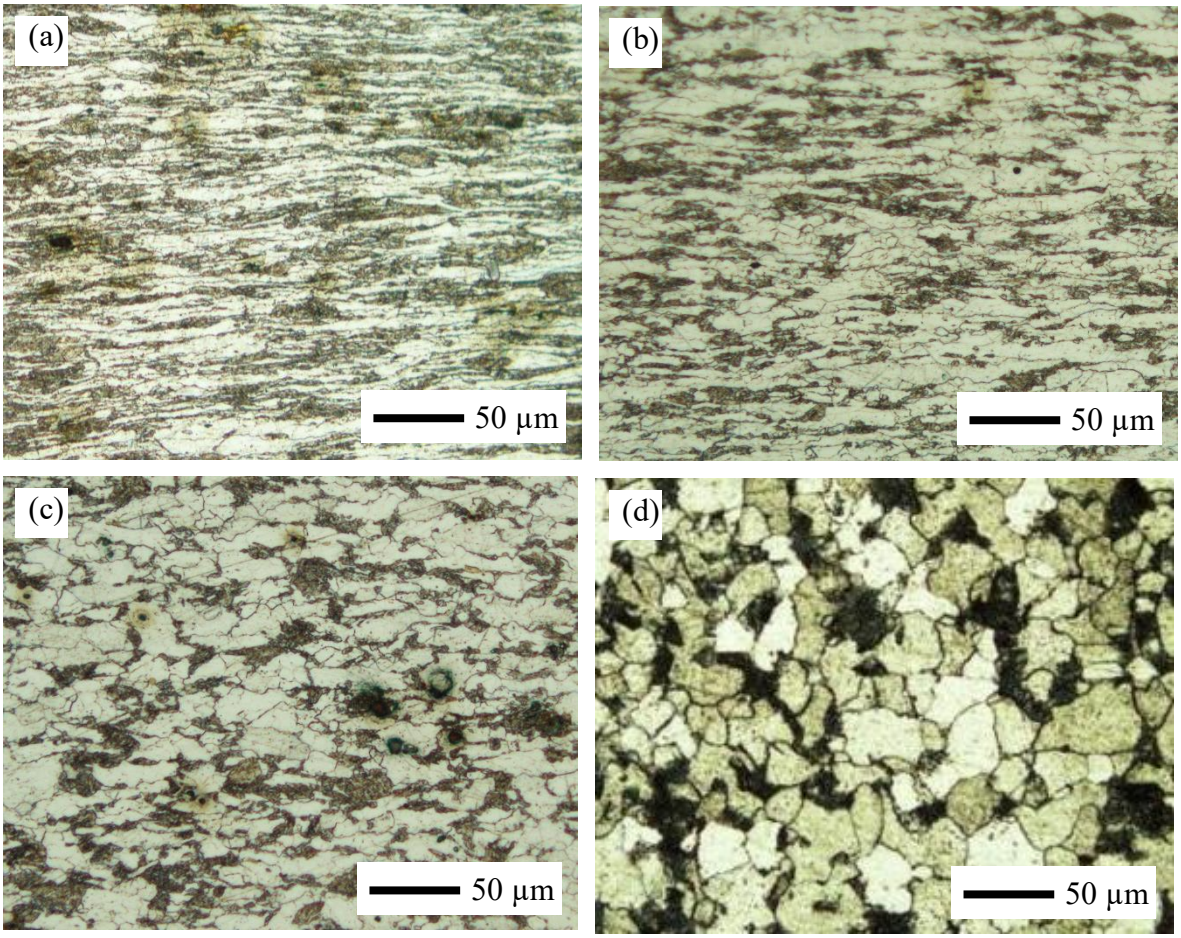

Figure 2. Optical microscope images of the ruptured tube at points (a) A, (b) B, (c) C and (d) the standard tube.

Table 2. Mechanical properties of the ruptured and the standard tube specimens

Tube	Brinell Hardness (HB)	Yield Strength (MPa)	Tensile Strength (MPa)
Standard	163	220	415
Rupture	213	337	512

In order to obtain a comprehensive analysis prior to the conclusion, a thorough microstructural examination using SEM was carried out to reveal whether there was a formation of a new phase or not.

Figure 3 presents the SEM images of the standard and ruptured tubes. The microstructure of the standard tube exhibited equiaxed grain consisting of the ferrite phase (α-Fe) and pearlite (α-Fe + Fe_3C), as shown in Figure 3 (a). This result is in agreement with Chandra et al., which found an elongated grain in the ruptured tube [22]. In addition, several pores were observed in the standard tube. In contrast, elongated grains with a high aspect ratio were formed in the ruptured tube, composed of ferrite and pearlite (Figure 3 (b)). This result is consistent with the optical microscope image in Figure 2(a). Interestingly, several cracks were found in the ruptured tube, as shown in Figure 3(b). The crack was possibly originated from the pores, which were elongated and then propagated because of high stress. EDS analysis of Figures 3(a) and 3(b) is shown in Table 3. The results show that the ruptured tube contained higher carbon content than the standard tube. The hardness increment of the ruptured tube can also occur due to higher carbon content in cementite. Thus, the ruptured specimen's hardness and strength increase due to the formation of the elongated grain and the cementite phase. Another interesting from EDS analysis was O detection in the ruptured tube, as shown in Table 3. It indicates that the tube experiences oxidation, which is characterized by the presence of O. Indeed, there is a weight increase because of the formation of a new oxide phase during oxidation, as reported by Aryanto et al. [23,24].

Since the change of material properties was also influenced by the operational parameter of a tube, a thorough inspection was also required. The diameter and the thickness of the standard tube were measured 57.1 and 9.27 mm, respectively. The tube's steam pressure and temperature during the normal operation were 144 ± 14.5 kg/cm^2 and 525 ± 14.5 °C, respectively. From the calculation using Equation (1), the hoop stress for the normal operation was 43.49 MPa, which was lower than the allowable stress of 60.2 MPa for SA213T22 at 525°C [8]. In contrast, during overheating, the steam pressure and the temperature were elevated to 167 kg/cm^2 and 605.5 °C, respectively, resulting in the hoop stress of 50.71 MPa. This hoop stress was almost two times higher than the allowable stress 32.9 MPa for SA213T22 at 600 °C. Therefore, this exceeded stress was the main cause of the failure, as indicated by the presence of the elongated grain and the crack propagation in the ruptured tube.

In this case, the degradation of material causing the tube breakage after 26 working hours occurred due to overheating and overpressure at a specific location. The overheating and excessive pressure took place in the operation due to the clogging of the fluid stream within the tube, leading to the anomaly in the fluid circulation.

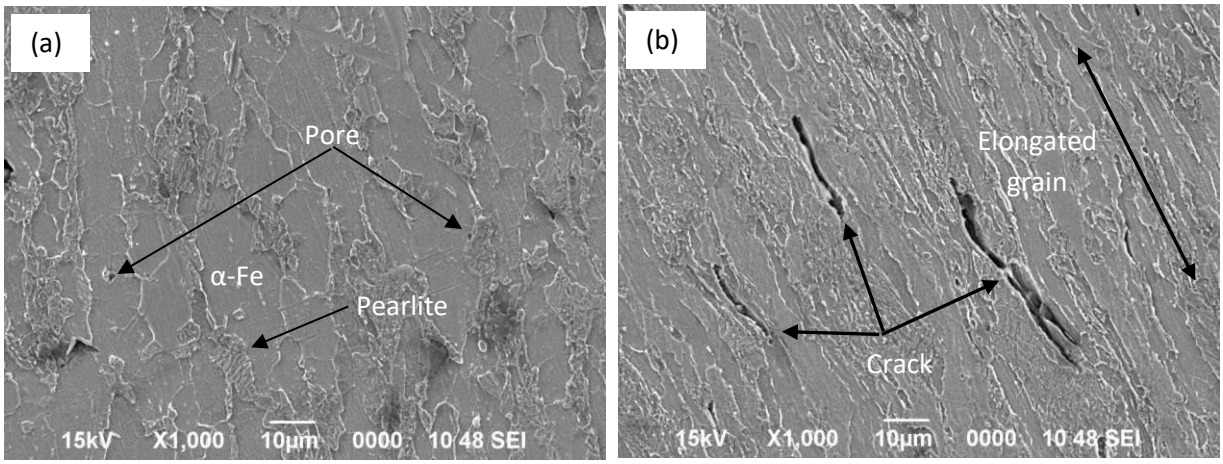

Figure 3. SEM images of (a) the standard tube and (b) the ruptured tube.

Table 3. Energy dispersive analysis of the tubes from Figures 3 (a) and (b)

	Fe (wt. %)	Cr (wt. %)	C (wt. %)	O (wt.%)	Others (wt. %)
Standard tube	91.96	2.23	3.50	-	2.31
Ruptured tube	82.83	2.11	8.31	6.75	-

Moreover, overheating and overpressure can also be initiated by overfiring the furnace at specific locations, producing excessive temperature rise.

The early degradation during the boiler start-up can be avoided by controlling the flow rate of the fluid stream; meanwhile, the clogging problem can also be overcome by using a boiler management system to improve the firing efficiency of the boiler. In addition, cleansing the crust in the furnace should be scheduled, as the presence of crust and ash deposits leads to incomplete flue gas flows, increasing the tube's temperature. Aljohani et al. developed a model using ANSYS to determine the wall temperature which related with deposit thickness in the tube for the prevention of failure [25]. Furthermore, regular inspection of the material properties should be conducted regularly, both on-site and in the laboratory. This inspection is important to predict the remaining lifetime of the material. By carrying out these approaches, inspection, maintenance, and replacement of the old tube can be well-planned. Therefore, the period of boiler tube termination can be predicted and mitigated.

CONCLUSION

The failure analysis of the tube material made of low carbon steel 2.25Cr-1Mo on the boiler secondary superheater (SSH) unit had been successfully investigated. The main cause of a tube's failure was excessive hoop stress, which was almost two times higher than the allowable stress. The hoop stress was 43.49 and 50.71 MPa in normal and overheating conditions. The stress due to overheating changed the microstructure from equiaxed to elongated grain, which subsequently increased the mechanical properties of the tube. Moreover, precipitation of the carbide at the grain boundaries and the presence of pores were favorable to initiate the crack. Therefore, controlling the fluid stream, boiler management system, and the crust's cleansing is imperative to prevent overheating as the main factor that induces the failure of the tube.

ACKNOWLEDGMENT

We thank PT. Sinergi Nanotech Indonesia for for providing the sample of ruptured tube and its characterization.

REFERENCES

[1] A. H. Assefinejad, A. Kermanpur, A. M. Eslami, and J. Kangazian, “Failure investigation of water wall tubes in a drum boiler of a thermal power plant,” *Engineering Failure Analysis*, vol. 118, ID: 104869, March 2020,doi:10.1016/j.engfailanal.2020.104869.

[2] M. A. Rahman et al., “Modelling the causes of boiler accidents: implications for economic and social sustainability at the workplace”, *Heliyon*, vol. 8, no. 6, ID: e09601, 2022, doi: 10.1016/j.heliyon.2022.e09601.

[3] S. Xue *et al.*, “Analysis of the causes of leakages and preventive strategies of boiler water-wall tubes in a thermal power plant,” *Engineering Failure Analysis*, vol. 110, ID: 104381, January 2020, doi: 10.1016/j.engfailanal.2020.104381.

[4] R. K. Hosseini and S. Yareiee, “Failure analysis of boiler tube at a petrochemical plant,” *Engineering Failure Analysis*, vol. 106, ID: 104146, February 2019, doi: 10.1016/j.engfailanal.2019.104146.

[5] M. A. Rao, R. S. Babu, and M. V. P. Kumar, “Stress corrosion cracking failure of a SS 316L high pressure heater tube”, *Engineering Failure Analysis*, vol. 90, pp. 14-22, 2018, doi: 10.1016/j.engfailanal.2018.03.013.

[6] A. Varma and R. K. Yadavalli, “Failure analysis of a reheater tube dissimilar metal weld failure in a 500 MW power plant”, *Engineering Failure Analysis*, vol. 118, ID: 104851, 2020, doi: 10.1016/j.engfailanal. 2020.10485.

[7] X. Liu et al. “Failure analysis and prediction based on corrosion thinning behaviour of atmospheric tower top and volatilization line connection area”, *Engineering Failure Analysis*, vol. 131, ID: 105914, January 2022, doi: 10.1016/j.engfailanal.2021.105914.

[8] P. Munda et al., “Evolution of Microstructure During Short-term Overheating Failure of a Boiler Water Wall Tube Made of Carbon Steel”, *Journal of Failure Analysis and Prevention*, vol. 18, no. 1, pp. 199–211, 2018, doi: 10.1007/s11668-018-0394-8.

[9] M. Awwaluddin et al., “Failure analysis of boiler leakage due to caustic corrosion on Cr-Mo steel”, *IOP Conference Series: Materials Science and Engineering*, vol. 536, no. 1, 2019, doi: 10.1088/1757-899X/536/1/ 012020.

[10] R. Sui et al., "Failure analysis of leakage at tube-to-tubesheet joints of a waste heat boiler", *Engineering Failure Analysis*, vol. 129, ID: 105639., 2021, doi: 10.1016/j.engfailanal.2021.105639.
[11] H. Ardy et al., "Failure Analysis of Bank-Wall Side Boiler Tube in a Petrochemical Plant," *Metals*, vol. 12, no. 12, ID. 2064, 2022, doi: 10.3390/met12122064.
[12] Y. S. Kim, W. C. Kim, J. Jain, E.-W. Huang, and S. Y. Lee, "Hydrogen Embrittlement of a Boiler Water Wall Tube in a District Heating System," *Metals*, vol. 12, no. 8, ID. 1276, 2022, doi: 10.3390/met12081276.
[13] M. Hong et al., "Failure Analysis of a Water Wall Boiler Tube for Power Generation in a District Heating System," *Metals and Materials International*, vol. 25, pp. 1191-1201, 2021, doi: 10.1007/s12540-019-00267-6.
[14] E. M. Zahrani, "Premature Failure of Grade-316Ti Stainless Steel Tubing in a Boiler Feed-Water Heat Exchanger in a Steel Complex," *Journal of Failure Analysis and Prevention*, vol. 21, pp. 61-73, 2021, doi: 10.1007/s11668-020-01037-y.
[15] Pramanick, A. K. et al., "Failure investigation of super heater tubes of coal fired power plant", *Case Studies in Engineering Failure Analysis*, vol. 9, pp. 17–26, October 2017, doi: 10.1016/j.csefa.2017.06.001.
[16] J. Li et al., "Failure analysis of the water-wall tube in KIVCET waste heat boiler", *Engineering Failure Analysis,* vol. 121 ID.105155, 2021, doi: 10.1016/j.engfailanal.2020.105155.
[17] A. Raja et al., "Effect of Grain Size on Superplastic Deformation of Metallic Materials", in *IntechOpen,* pp. 1–22, 2019, doi: 10.5772/intechopen.86017.
[18] V. I. Kopylov et al., "Effect of σ-Phase on the Strength, Stress Relaxation Behavior, and Corrosion Resistance of an Ultrafine-Grained Austenitic Steel AISI 321," *Metals*, vol. 13, no. 1, ID. 45, 2023, doi: 10.3390/met13010045.
[19] A. V. Mikhaylovskaya et al., "Comparison between superplastic deformation mechanisms at primary and steady stages of the fine grain AA7475 aluminium alloy," *Materials Science and Engineering: A*, vol. 718, pp. 277-286, 2018, doi: 10.1016/j.msea.2018.01.102.
[20] O. Reck and R. Pippan, "Saturation of Grain Refinement during Severe Plastic Deformation of Single Phase Materials: Reconsiderations, Current Status and Open Questions," *Materials Transactions*, vol. 60, no. 7 pp. 1270-1282, 2019, doi: 10.2320/matertrans.MF201918.
[21] Y. S. Kim, W. C. Kim, and J. G. Kim, "Bulging rupture and caustic corrosion of a boiler tube in a thermal power plant", *Engineering Failure Analysis*, vol. 104, pp. 560–567, 2019, doi: 10.1016/j.engfailanal.2019.06.022.
[22] B. Haghighat-Shishavan et al., "Failure analysis of a superheater tube ruptured in a power plant boiler: Main causes and preventive strategies", *Engineering Failure Analysis*, vol. 98, pp. 131–140, 2019, doi: 10.1016/j.engfailanal.2019.01.016.
[23] D. Aryanto *et al.*, "Effect of annealing temperature on the oxidation behavior of ferrosilicon-aluminum-coated low carbon steel by mechanical alloying," *Journal of Alloys and Compounds*, vol. 821, ID: 153493, 2020, doi: 10.1016/j.jallcom.2019.153493.
[24] D. Aryanto *et al.*, "Microstructure and oxidation behavior of an Al–Ni–Cr–Cu–MoO_3–SiO_2 composite coating on low-carbon steel," *Materials Chemistry and Physic*, vol. 261, ID: 124250, 2021, doi: 10.1016/j.matchemphys.2021.124250.
[25] A. S. Aljohani *et al.*, "Numerical Study on the Effect of Deposit Layer on the MinimumWall Thickness of Boiler Water Tube under Different Operating Conditions," *Applied Sciences*, vol. 12, ID: 8838, 2022, doi: 10.3390/app12178838.